An *ab initio* study of the magnetic–metallic $CoPt_3$–Au interfaces

2009 J. Phys.: Condens. Matter 21 015001

(http://iopscience.iop.org/0953-8984/21/1/015001)

IOP PUBLISHING JOURNAL OF PHYSICS: CONDENSED MATTER

J. Phys.: Condens. Matter **21** (2009) 015001 (13pp) doi:10.1088/0953-8984/21/1/015001

An *ab initio* study of the magnetic–metallic $CoPt_3$–Au interfaces

Letizia Chiodo[1], **Fabio Della Sala, Teresa Pellegrino, Roberto Cingolani and Liberato Manna**

NNL-National Nanotechnology Laboratories of CNR-INFM, Via Arnesano, 73100, Lecce, Italy

E-mail: letizia.chiodo@unile.it

Received 7 July 2008, in final form 25 October 2008
Published 1 December 2008
Online at stacks.iop.org/JPhysCM/21/015001

Abstract

The new challenging field of fabrication and interconnection of inorganic nanostructures is giving new impetus to the study of solid–solid interfacial properties. In nanocrystals made of two domains of different chemical composition and sharing an interface, the interfacial behavior is indeed critical for the stability of such an interface, and also in determining the mutual interactions of the two domains. Following a recent study by our group on the growth of colloidal nanocrystal heterodimers made of a domain of Au and a domain of $CoPt_3$, we report here an *ab initio* density functional theory study of the structural and electronic properties of Au/$CoPt_3$ interfaces. We have investigated the structure of different bulk $CoPt_3$ facets and of Au atoms adsorbed on $CoPt_3$. We calculated $CoPt_3$ and Au surface energies, Au/$CoPt_3$ interfacial energies as well as adsorption energies of Au atoms on $CoPt_3$ and Au, and we can draw some important conclusions about the growth mechanism of gold on the magnetic alloy. Furthermore, we give here a detailed description of surface and interfacial electronic properties, which in turn determine the possibility of tuning conductivity and magnetic properties in the nanostructure.

(Some figures in this article are in colour only in the electronic version)

1. Introduction

The theoretical investigation of solid–solid interfaces is of fundamental importance in several areas of research and technology. In solid state device physics, for instance, theoretical studies of interfaces have shed light on important issues such as polarization and band offsets at semiconductor–semiconductor interfaces [1–6]. The study of solid–solid interfaces is also of crucial relevance in the emerging field of fabrication of inorganic nanostructures and of their integration into optical, electronic and magnetic devices [7]. In materials chemistry, one recent exciting direction is represented by the development of colloidal inorganic nanocrystals that can be synthesized with control over their size, shape and chemical composition [7, 8]. Such nanocrystals are now reaching a high level of complexity as they start integrating different domains of various inorganic materials, which are often attached together through specific crystallographic facets and therefore evolve via the formation of well-defined solid–solid interfaces [8]. Understanding the parameters that govern such interfaces represents an important step towards greater control over the synthesis of novel combinations of materials and ultimately towards modeling and tailoring their physical and chemical properties.

The study of interfacial solid structures is, however, not an easy task. Nowadays there are only a few experimental techniques by which it is possible to investigate the structural properties of interfaces between two solids, and many of them rely on transmission electron microscopy (TEM) [9, 10]. *Ab initio* calculations of interfaces are not straightforward due the high computational costs and the difficulty of determining a good starting configuration for the atomic structure of the interface, which is often characterized by the build-up of strain, the formation of dislocations as well as by the occurrence of deformations, reconstructions and atomic substitutions. In nanocrystals, due to their topology and finite size, deformations and defects can be expected to be more frequent than in epitaxially grown crystals. Moreover, the

[1] Author to whom any correspondence should be addressed. Present address: Nano-Bio Spectroscopy group and European Theoretical Spectroscopy Facility (ETSF), Dpto. de Física de Materiales, Universidad del País Vasco UPV/EHU and Centro Mixto CSIC-UPV/EHU, Av. Tolosa 72, E-20018 San Sebastián, Spain.

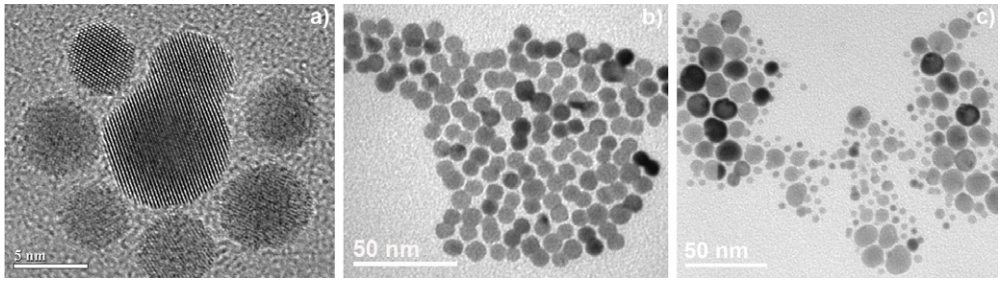

Figure 1. Transmission electron microscopy (TEM) images of $CoPt_3$–Au nanocrystal heterodimers. Panel (a) shows a high-resolution image of a heterodimer surrounded by unreacted $CoPt_3$ nanocrystals. The large domain in the heterodimer is made of gold. Panels (b) and (c) report wide field, low-magnification images of symmetric and strongly asymmetric heterodimers, respectively. In panel (c) the small, isolated spherical domains are again unreacted $CoPt_3$ nanocrystals.

computation of surface and/or interfacial energies is highly sensitive to numerical parameters such as slab thickness and *k*-point sampling [11]. Due to these intrinsic difficulties, *ab initio* calculations of structural and electronic properties of interfaces have so far mainly targeted semiconductors [1–6], due to the importance of band offset determination in traditional inorganic electronic devices. Recently several examples of different interfaces have been proposed [12–17], including metal–ceramics [18, 19], metal–semiconductor systems for spintronics [14] and interfaces of transition metals, nitrides and carbides with metal oxides [20]. The most common computational approach to study metal–metal interfaces relies on the embedded atom method [21], which is less computationally expensive than *ab initio* density functional (DFT) calculations.

We report here the results of *ab initio* DFT calculations on interfaces between the magnetic stoichiometric alloy $CoPt_3$ and gold. These calculations focus on two main topics: the identification of the most stable alloy configurations for $CoPt_3$, which we achieved by analyzing the relaxation and rearrangement of the surface layers and the surface energies of different $CoPt_3$ facets; and the analysis of gold–alloy growth and interaction, through the calculation of adsorption and interfacial energies for different $CoPt_3$–Au interfaces. While gold surfaces have been investigated more thoroughly, in particular concerning the (111) orientation, for $CoPt_3$ surfaces only experimental results have been reported so far, and a theoretical analysis of facet stability is still lacking. We found that the most unstable, and therefore the most reactive, orientation is the (110) one for both $CoPt_3$ and clean Au surfaces. The energetic situation becomes somehow more elaborate when interfaces are considered.

The major drive for this study comes from the recently reported synthesis of colloidal heterodimers of $CoPt_3$–Au by our group [22]. These heterodimers (see figure 1) were prepared by a two-step procedure in which $CoPt_3$ nanocrystals were first grown, and later Au was nucleated on them [22]. In general, Au magnetic bi-functional nanocrystals might find applications in biomedicine, as the magnetic domain could be exploited as a means to enhance the contrast and the resolution in magnetic resonance imaging and also to induce local hyperthermia [23, 24], while the Au domain might serve as a preferential anchoring region for a wide range of biomolecules and additionally might be used to elicit hyperthermia locally [25–27].

One peculiar feature of the growth of Au on colloidal $CoPt_3$ nanocrystals reported by our group is that Au does not entirely 'wet' the starting $CoPt_3$ nanocrystal but rather forms a separate spherical domain, which is epitaxially attached to the former nanocrystal [22]. In such a heterodimer (see figure 1) the two Au and $CoPt_3$ domains can share one of the (100), (110) or (111) facets. Another peculiarity that we reported in our synthesis work [22] was that Au seemed to prefer growth over the (111) facet of the $CoPt_3$ nanocrystals, at least for small (diameter less than 3 nm) $CoPt_3$ nanocrystals. The formation of heterodimers occurred even if large amounts of Au chemical precursors were introduced into the reaction environment. In that case, remarkably asymmetric $CoPt_3$–Au heterodimers were synthesized, in which the attached Au domain was much larger than the $CoPt_3$ domain (see figures 1(a) and (c)). This is clearly different from several reports on colloidal core/shell (i.e. onion-like) nanostructures which were either the result of a uniform epitaxial shell of a second material that had grown on top of the starting nanocrystal [28–31], or more frequently of a polycrystalline shell arising from nucleation and partial coalescence of various domains on different facets of the starting nanocrystal [32–35]. The *ab initio* calculations reported in this work focus on the identification of the most stable alloy configurations for $CoPt_3$, on the relaxation and rearrangement of the surface layers, on the calculation of surface energies of different $CoPt_3$ facets as well as on the calculation of interfacial energies for different $CoPt_3$–Au interfaces. We also report on electronic and magnetic modifications induced on the materials by the asymmetry due to the surface and the interface formation.

In the following analysis and discussion of theoretical results, some important points must be kept in mind: (i) we are studying infinite and perfect surfaces and interfaces, therefore we cannot include the relaxations, kinks and strains present in real, finite interfaces between nanocrystalline domains; (ii) we are modeling the pre-existing magnetic nanocrystal by keeping its in-plane structure unaffected by the Au adsorption; (iii) our model holds for a growth in ideal conditions, i.e. a vacuum and 0 K: all the effects of surfactants and solvents involved in solution growths on both $CoPt_3$ and Au energetic balance and growth mechanisms have not been taken into account;

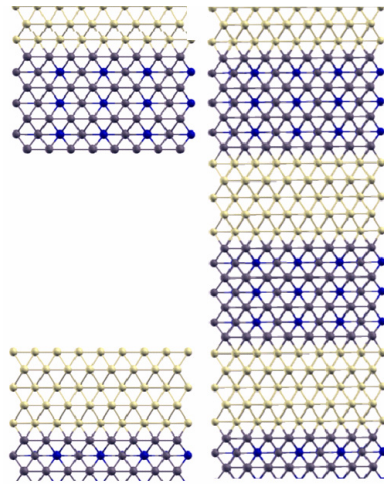

Figure 2. Model supercells used for the interface calculations [39]. Left, supercell with a vacuum region; right, continuum supercell. The yellow (light) atoms represent gold, the blue-gray (black-dark) atoms the $CoPt_3$ alloy.

(iv) finally we are totally disregarding the effect of temperature on growth, because we are performing our calculations at $T = 0$ K, for an equilibrium system, while the dimer growth is carried out at much higher temperatures (at ∼330 K), out of thermodynamic equilibrium.

The paper is organized as follows: after a description of the theoretical methods in section 2 and of the computational details in section 3, we report in section 4 the structural and the energetic properties of the $CoPt_3$ and Au facets, the Au atomic adsorption on $CoPt_3$ facets and the results for Au/$CoPt_3$ interfaces. Section 5 reports the electronic and magnetic structure of the heterointerfaces and in section 6 we discuss the growth of gold on $CoPt_3$ facets based on the *ab initio* results for the relative stabilities of various systems.

2. Theoretical methodology

2.1. General considerations

Bulk $CoPt_3$ is structurally ordered but chemically disordered above 685 °C (disordered fcc phase), and becomes chemically ordered (fcc *Ll*2 phase) below 685°C [36]. In the present work we considered ordered structures, mainly for the sake of much reduced computational costs. $CoPt_3$ and Au share the same fcc crystal structure, therefore we can define interfaces between the two materials with the same crystal orientation. Because we are modeling the growth of Au on pre-synthesized colloidal $CoPt_3$ nanocrystals, we apply an in-plane strain to the growing gold.

We first analyze the clean $CoPt_3$(001), $CoPt_3$(110) and $CoPt_3$(111) facets, and the corresponding Au facets, then we describe the adsorption of single Au atoms or of a single Au monolayer on $CoPt_3$ facets. Finally we study the complex interfaces between $CoPt_3$ and gold.

We have used the repeated supercell method to model all the considered interfaces (see figure 2), as is often done for describing extended surfaces and interfaces [21, 37, 38].

Table 1. Vertical relaxation of the three high symmetry $CoPt_3$ facets (rows I–III), with respect to the bulk-truncated ones, and of interface structures (IV–VI), with respect to the ideal bulk-truncated surface. The columns contain the relaxation of the third (Δd_3) second (Δd_2), and first (Δd_1), $CoPt_3$ layer positions, respectively, the relaxation of the Au–surface distance $\Delta d_{\mathrm{Au-surface}}$, and of the second Au layer position $\Delta d_{\mathrm{Au-Au}}$. A buckling of 0.05–0.08 Å has been observed in the first surface layer of the alloy.

	Δd_3 (%)	Δd_2 (%)	Δd_1 (%)	$\Delta d_{\mathrm{Au-surface}}$ (%)	$\Delta d_{\mathrm{Au-Au}}$ (%)
(111)	+1.2	−3.1	−0.3		
(001)	−0.3	−3.8	−4.6		
(110)	−2.2	+8.4	−15.6		
(111)	+2.9	−4.4	+0.7	+3.0	+7.9
(001)	−0.8	−3.5	−6.1	+5.8	+7.6
(110)	−0.8	+0.7	−3.9	+3.9	+7.9

The clean facets of both $CoPt_3$ and Au were modeled by five-, seven- and nine-layer thick slabs, with a (2×2) surface unit cell for $CoPt_3$, in order to reproduce the correct surface stoichiometry, and by a vacuum region that is six layers thick (corresponding to 13.1, 8.1, and 11.4 Å for the three (111), (110) and (001) $CoPt_3$ facets, respectively, and to 14.0, 8.6 and 12.2 Å for the corresponding Au facets). The (111) interface was modeled by a slab containing $6(CoPt_3) + 6$(Au) layers, while the (110) and the (001) interfaces were modeled by a slab containing $7(CoPt_3) + 7$(Au) layers. In all cases the (2×2) surface cell geometry was preserved.

The vacuum region is used in supercell calculations to ensure convergence of the calculation of surface properties, such as atomic relaxation and surface energies. For $CoPt_3$, different local surface geometries were considered based on the different locations of the Co atoms in the crystal lattice of the alloy, in order to identify the most stable configurations of surface atoms. In all our calculations, relaxed but non-reconstructed surface models were used, and we disregarded dislocations, contaminations, and inter-diffusion, as well as the presence of surfactants, which in principle can affect the surface energetics [40, 41]. The various interfaces (see below) were built by assuming for Au, in the directions parallel to the interface, the same theoretical lattice constant as for $CoPt_3$, while the calculated Au lattice constant was used in the direction of the epitaxial growth, normal to the interface. The structure perpendicular to the interface was further allowed to relax (see table 1). As a consequence of this choice for the lattice parameters of Au along different crystallographic directions, in all the interfacial calculations reported here Au is assumed to have a tetragonal phase.

2.2. Adsorption energies

Let us define E_{tot}(Au) as the energy of the Au atom (calculated either for an atom in a bulk crystal or for an isolated atom), n as the number of Au atoms that form one monolayer (ML) on the surface unit cell, $E_{\mathrm{tot}}(CoPt_3\ \mathrm{slab})$ as the energy of the $CoPt_3$ slab and E_{tot} as the energy of the adsorbate/substrate system. The adsorption energy E_{ads} of a single Au atom on the generic $CoPt_3$ facet is then defined as

$$E_{\mathrm{ads}} = [E_{\mathrm{tot}}(\mathrm{Au}) + E_{\mathrm{tot}}(CoPt_3\ \mathrm{slab})] - E_{\mathrm{tot}}. \qquad (1)$$

The adsorption energy $E_{\mathrm{ads-ML}}$ of a single Au atom within 1 ML on the generic $CoPt_3$ facet is defined instead as:

$$E_{\mathrm{ads-ML}} = [[n \cdot E_{\mathrm{tot}}(\mathrm{Au}) + E_{\mathrm{tot}}(\mathrm{CoPt_3\ slab})] - E_{\mathrm{tot}}]/n. \quad (2)$$

Positive values of E_{ads} and $E_{\mathrm{ads-ML}}$ mean that a bond is created.

2.3. Surface energies

The key quantity of this study is the surface energy. We recall that in this description we are not considering the full thermodynamic treatment as we are neglecting vibrational contributions, we are replacing the Gibbs free energy with the DFT total energy [4], and in addition we are only dealing with the zero temperature surface energy [42]. Within these approximations, for a given facet, the surface energy is extracted from a total energy calculation on the slab that exposes that specific facet. A slab always exposes a top and a bottom facet, and for a binary compound such as $CoPt_3$, the sum of the top (σ_{top}) and bottom (σ_{bottom}) surface energies of the top and bottom facets per supercell is defined as

$$\sigma_{\mathrm{top}} + \sigma_{\mathrm{bottom}} = E_{\mathrm{tot}}(\mathrm{slab}) - n_{\mathrm{Co}} \cdot \mu_{\mathrm{Co}} - n_{\mathrm{Pt}} \cdot \mu_{\mathrm{Pt}}. \quad (3)$$

$E_{\mathrm{tot}}(\mathrm{slab})$ is the total energy of the slab, n_{Co} and n_{Pt} are the numbers of Co and Pt atoms in the slab and μ_{Co} and μ_{Pt} are their respective chemical potentials in bulk $CoPt_3$. In the present case (and also for calculations involving Au), due to the cubic symmetry of the lattice we can build up slabs for which $\sigma_{\mathrm{top}} = \sigma_{\mathrm{bottom}} = \sigma$ and therefore the previous expression can be simply written as

$$2\sigma = E_{\mathrm{tot}}(\mathrm{slab}) - n_{\mathrm{Co}} \cdot \mu_{\mathrm{Co}} - n_{\mathrm{Pt}} \cdot \mu_{\mathrm{Pt}}. \quad (4)$$

The surface energy per unit area is obtained by dividing σ by the surface area A of the slab. For slabs exposing certain facets, in particular the (111) facet in the present case, the stoichiometric Co:Pt ratio is the same as in the bulk (that is 1:3). In this simple case, the surface energy is unambiguously defined as

$$\begin{aligned} 2\sigma &= E_{\mathrm{tot}}(\mathrm{slab}) - N_{\mathrm{CoPt_3}} \cdot (\mu_{\mathrm{Co}} + 3\mu_{\mathrm{Pt}}) \\ &= E_{\mathrm{tot}}(\mathrm{slab}) - N_{\mathrm{CoPt_3}} \cdot E_{\mathrm{tot}}(\mathrm{CoPt_3}). \end{aligned} \quad (5)$$

Here $N_{\mathrm{CoPt_3}}$ represents the number of $CoPt_3$ 'molecules' present in the slab and $E_{\mathrm{tot}}(\mathrm{CoPt_3})$ can be evaluated straightforwardly from a bulk $CoPt_3$ calculation. For slabs exposing other facets, such as the (001) or the (110) facet, or in general for the various types of slabs that expose particular types of surfaces (i.e. Pt-rich ones), the Co:Pt stoichiometric ratio is unfortunately not the same as in the bulk $CoPt_3$ crystal and therefore the surface energies depend on the individual values of μ_{Co} and μ_{Pt}, which cannot be defined uniquely. Nevertheless, it is possible to evaluate the range of possible values for μ_{Co} and μ_{Pt} by calculating the chemical potentials for Co and Pt in their respective pure bulk solids, $E_{\mathrm{tot}}(\mathrm{Co})$ and $E_{\mathrm{tot}}(\mathrm{Pt})$. For $CoPt_3$ to be a stable compound, and therefore for the individual Co and Pt components not to separate from $CoPt_3$ to form their pure elemental solids, the following relations must hold for the chemical potentials μ_{Co} and μ_{Pt} in $CoPt_3$:

$$\mu_{\mathrm{Co}} \leqslant E_{\mathrm{tot}}(\mathrm{Co}) \quad (6)$$

$$\mu_{\mathrm{Pt}} \leqslant E_{\mathrm{tot}}(\mathrm{Pt}). \quad (7)$$

Moreover, we can use the following expression to define the enthalpy of formation of $CoPt_3$:

$$E_{\mathrm{tot}}(\mathrm{CoPt_3}) = E_{\mathrm{tot}}(\mathrm{Co}) + 3E_{\mathrm{tot}}\,(Pt) + \Delta H_f(\mathrm{CoPt_3}). \quad (8)$$

By merging the former equations with the equation $\mu_{\mathrm{Co}} + 3\mu_{\mathrm{Pt}} = E_{\mathrm{tot}}(\mathrm{CoPt_3})$ we can derive the following expression for the range of variation of μ_{Co} in $CoPt_3$:

$$E_{\mathrm{tot}}(\mathrm{Co}) + \Delta H_f(\mathrm{CoPt_3}) \leqslant \mu_{\mathrm{Co}} \leqslant E_{\mathrm{tot}}(\mathrm{Co}). \quad (9)$$

We will define the lower and upper values for μ_{Co} in $CoPt_3$ as those related to a Co atom in a Co-poor (minimum μ_{Co}) $CoPt_3$ crystal and in a Co-rich (maximum μ_{Co}) $CoPt_3$ crystal, respectively. In the slab calculations involving Au, on the other hand, surface energies are always defined unambiguously as

$$2\sigma = E_{\mathrm{tot}}(\mathrm{slab}) - n_{\mathrm{Au}} \cdot \mu_{\mathrm{Au}}. \quad (10)$$

In the latter case μ_{Au} can be always determined directly by a 'bulk Au' calculation, since $\mu_{\mathrm{Au}} = E_{\mathrm{tot}}(\mathrm{Au})$.

For the real $CoPt_3$ and Au surfaces, the $E_{\mathrm{tot}}(\mathrm{X})$ (X = Co, Pt, Au) used are given by the optimized bulk system geometry.

2.4. Interfacial energies

The same principles can be applied to the calculation of interfacial energies for the $CoPt_3$–Au system. The determination of the various $CoPt_3$–Au interfacial energies can be made to a first approximation by constructing a repeated slab. The superlattice used is drawn in figure 2, right panel. This is formed by one thick section made of several layers that contain N_{Au} Au atoms that are sitting on top of another thick section made of several $CoPt_3$ layers, and this unit is repeated without vacuum sections. The interfacial energy *per* unit area is given by [17]

$$\gamma = \frac{E_{\mathrm{tot}}(\mathrm{slab}) - N_{\mathrm{Au}}E_{\mathrm{tot}}(\mathrm{Au}) - n_{\mathrm{Co}} \cdot \mu_{\mathrm{Co}} - n_{\mathrm{Pt}} \cdot \mu_{\mathrm{Pt}}}{2A}. \quad (11)$$

Here A represents the interfacial area shared by the two different materials per unit supercell and n_{Co}, μ_{Co} (n_{Pt}, μ_{Pt}) are the number of Co (Pt) atoms and their chemical potential in $CoPt_3$, respectively, and $E_{\mathrm{tot}}(\mathrm{slab})$ is the total energy of the full superlattice, which does not include a vacuum region. This expression is clearly valid only for interfaces that share the same crystal structure and the same crystallographic direction, which is certainly the case here. Like the surface energy, the interfacial energy is dependent on the chemical potential of Co (or Pt). If the $CoPt_3$ layer has the same stoichiometry as in the bulk, so that it contains $N_{\mathrm{CoPt_3}}$ 'molecules' of $CoPt_3$, the interfacial energy is defined unambiguously by the following expression:

$$\gamma = \frac{E_{\mathrm{tot}}(\mathrm{slab}) - N_{\mathrm{Au}}E_{\mathrm{tot}}(\mathrm{Au}) - N_{\mathrm{CoPt_3}}E_{\mathrm{tot}}(\mathrm{CoPt_3})}{2A}. \quad (12)$$

Table 2. *Ab initio* calculated surface and interfacial energies of the three high symmetry $CoPt_3$ and Au facets. For the alloy, results for both most the stable (first row) and least stable (second row) geometries are reported. For the (111) facet, the two configurations are shown in figures 3(a) and (b). In this case the highest stability is reached with an exchange of one Co atom from the top outermost layer with a Pt atom from the second outermost layer. For the (001) and (110) facets the most stable configurations are shown in figures 3(c) and (d), and correspond to real, bulk terminated surfaces, without any atomic substitution. For the (001) and (110) facets, lower and upper limits are given for their surface energy. *Ab initio* surface energies of gold (third row) are compared with experimental data (fourth row) and with previous calculations (fifth row). The sixth row reports the values for the in-plane strained Au facets, as in the case of Au grown on top of $CoPt_3$. The last row reports the $CoPt_3$–Au interfacial energies for the three high symmetry directions. For the (110) and the (001) interfaces only lower and upper limit values of interfacial energies can be defined.

σ (eV Å^{-2})	(111)	(001)	(110)
$\sigma^{\text{theo}}_{\text{CoPt}_3}$ (stable)	0.110	$0.13 \leqslant \sigma \leqslant 0.23$	$0.14 \leqslant \sigma \leqslant 0.20$
$\sigma^{\text{theo}}_{\text{CoPt}_3}$ (unstable)	0.130	$0.200 \leqslant \sigma \leqslant 0.280$	$0.14 \leqslant \sigma \leqslant 0.20$
$\sigma^{\text{theo}}_{\text{Au}}$	0.069	0.081	0.088
$\sigma^{\text{exp}}_{\text{Au}}$	0.065	0.081	—
$\sigma^{\text{theo}}_{\text{Au}}$ (other works)	0.047 [46]	0.078 [62]	0.091 [63]
$\sigma^{\text{theo}}_{\text{Au}}$ (strained)	0.049	0.077	0.053
$\gamma_{\text{Au/CoPt}_3}$ (eV Å^{-2})	0.012	$-0.015 \leqslant \gamma \leqslant 0.063$	$0.012 \leqslant \gamma \leqslant 0.067$

We aim at simulating the magnetic substrate of the pre-existing nanocrystals by keeping constant the in-plane cell dimensions of $CoPt_3$ when Au is adsorbed on it. One complication of this study arises from the significantly large difference in lattice parameters between the $CoPt_3$ and Au, which is about 6.2% according to experimental data [43–46] (we computed a 6.3% lattice mismatch). As a consequence of this lattice mismatch, the epitaxial growth of Au on top of $CoPt_3$ will be highly strained and this strain must be included somehow in the energetic study of the interface. In order to do so, we have followed a two-step approach. First, the Au–$CoPt_3$ interface was modeled with a two-material slab sandwiched by a vacuum (figure 2, left panel). The overall supercell was therefore formed by an isolated slab that includes an interface, two vacuum-exposed surfaces and a vacuum region (see figure 2, left panel). Calculations run on such a supercell aimed to establish a satisfactory arrangement of gold atomic positions close to the interfacial region. We can expect that $CoPt_3$, and especially Au, relax in the direction perpendicular to the interface, since Au is compressed in the plane parallel to the interface. If σ_{CoPt_3} and σ_{Au} are the surface energies per unit area of the vacuum-exposed $CoPt_3$ and Au facets, respectively, and A is the interfacial area per supercell, one can define the $CoPt_3$–Au interfacial energy γ per unit area as

$$\gamma + \sigma_{\text{CoPt}_3} + \sigma_{\text{Au}} = \frac{E_{\text{tot}}(\text{slab}) - N_{\text{Au}} E_{\text{tot}}(\text{Au}) - N_{\text{CoPt}_3} E_{\text{tot}}(\text{CoPt}_3)}{A}. \quad (13)$$

Here E_{tot}(slab) is the energy of the supercell including a $CoPt_3$–Au slab and vacuum. In the former expression the interfacial energy depends on the surface energies of the two vacuum-exposed facets, which might be affected by the type of surface passivation, by errors and by additional parameters. A better estimate of the interfacial energy is therefore made by building a fully solid repeated slab (see figure 2, right panel) without any vacuum region and by using as parameters for the atomic positions close to the $CoPt_3$–Au interface those that were determined in the previous step with the vacuum-sandwiched slab. In this way, γ can be directly evaluated from total energy values (equations (11) and (12)), therefore avoiding the need of including σ_{CoPt_3} and σ_{Au} in the calculations, along with their associated errors.

A further detail to be taken into account is the inclusion of the strain energy contribution. Given the difference in lattice constant between the two materials, the calculation of γ is performed by using for the energy of bulk gold the value obtained by imposing the same lateral lattice constraint as for the grown ad-layers (epitaxial lattice constant), and by allowing relaxation along the third direction, starting from the natural gold lattice constant evaluated for the cubic fcc bulk phase. In this way, the stress contribution is included in the bulk term, which is different for each crystallographic orientation, and removed by the γ values. For the bulk energy of $CoPt_3$, the real relaxed one is retained because we assumed that no stress has been applied to the magnetic substrate.

3. Computational details

Ab initio spin polarized calculations were carried out in the framework of DFT [47, 48], using the plane-waves code PWSCF [49]. The local density approximation (LDA) in the Perdew–Zunger [50] parameterization and the local spin density approximation (LSDA) [51] for the exchange–correlation potential have been considered [52].

We also performed test calculations for lattice constants and magnetic moments at the GGA level for bulk hcp-Co, bulk fcc-Co and bulk $CoPt_3$. For $CoPt_3$ the GGA lattice constant is 3.91 Å, much larger than the experimental results and the LDA values (see section 4.1). Indeed it has been shown [53] that LDA is slightly superior to GGA in describing the structural properties of both Pt and Au, even in 2D systems such as surfaces, and gives results comparable to GGA for Co. We indeed obtain a good estimation of gold surface energies by LDA with respect to both experiment and GGA (see table 2). Moreover, GGA largely overestimates magnetic moments [52] (see table 4). For these reasons, the calculations for surfaces and interfaces have been performed at the LDA level.

The electronic configurations are Co $3d^8\ 4s^1$, Pt $5d^9\ 6s^1$ and Au $5d^{10}\ 6s^1$. Ultra-soft pseudopotentials [54] have been chosen, including scalar relativistic effects for all considered elements. To reduce the computational cost, we did not include a full relativistic description as we are mainly interested in energy differences between surfaces and interfaces with different orientations, which can be described quite accurately using scalar relativistic pseudopotentials.

A wavefunction and charge density cut-off of 40 and 240 Ryd are used, respectively, to ensure convergence on structural properties. Convergence on energy cut-off has been carefully checked for the $CoPt_3$ and the Au bulk systems, and we observed a convergence of 0.01 eV on total energies and of 0.001 eV on eigenvalues, using 120 k-points in the irreducible Brillouin zone (BZ). The electronic (density of states) and magnetic (magnetic moment) properties of the inner layer of the slab reproduce the bulk behavior, ensuring the slab thickness convergence. The largest cell used in this series of calculations includes 56 atoms. We performed supercell calculations using a Monkhorst–Pack mesh of up to $8\times8\times1$ k-points for the (2×2) surface cell. All the systems that we modeled were allowed to relax under forces calculated by the Hellmann–Feynman approach, until Cartesian force components per atom were lower than 0.025 eV $Å^{-1}$.

4. Results

4.1. The $CoPt_3$ and Au facets

Preliminary bulk calculations give for the $CoPt_3$ stoichiometric alloy a lattice constant $a = 3.82$ Å (3.80 Å for paramagnetic calculation), in good agreement with the old experimental value of 3.83 Å [43] and with the newest 3.85 Å [44, 45] found for the ordered phase of the alloy. The calculated lattice parameter of Au (4.05 Å) is also in rather good agreement with the experimental value of 4.08 Å [46]. The slight theoretical underestimation of lattice constants is a well known effect of the LDA [55].

It is known experimentally [36] that the lower surface energy of pure Pt with respect to pure Co induces pure Pt termination on both (111) and (001) facets (see figures 3(a)–(c)), but not on the (110) facet (see figure 3(d)). The reason for this might be that magnetic atoms prefer to be embedded inside the alloy and not to stay at surface sites (an effect known as positive segregation energy) [56].

We start our theoretical analysis with the $CoPt_3(111)$ facet, which is expected to be the most stable one for $CoPt_3$ due to its close-packed arrangement [36]. The ideal bulk-truncated surface is built up by one Co and three Pt atoms, while the lowest-energy termination, experimentally observed [36, 45], and here theoretically verified, is based on a pure Pt surface in which one Co atom from the top outermost layer has been exchanged with one Pt atom from the second layer (see figures 3(a) and (b)). Our calculations show that the Pt-terminated facet is more stable than the bulk-truncated one by 0.270 eV/(surface atom). For the paramagnetic case we obtain 0.265 eV/(surface atom).

The bulk-truncated $CoPt_3(001)$ facet can expose either a pure Pt (see figure 3(c)) or a half-Pt–half-Co plane, but the pure Pt one is experimentally found to be energetically preferred [36]. Also this result was confirmed by our calculations, by computing the surface energy difference between the pure Pt and the half-Pt–half-Co surface. For this facet we used the ideal unreconstructed symmetry and did not consider in the calculations the experimentally observed quasi-hexagonal reconstruction [57], due to the high computational cost of including reconstruction in the present calculations. For slabs exposing this type of facet it should be noted that the system has a stoichiometry that depends on the number of material layers, and which in general differs from the $CoPt_3$ bulk stoichiometry (see section 2). The evaluation of the stability of this facet, as mentioned before, involves knowledge of the chemical potentials of bulk Pt and bulk Co, and therefore our calculations cannot give an unambiguous value but rather a range of values, which depend on μ_{Co} and μ_{Pt}.

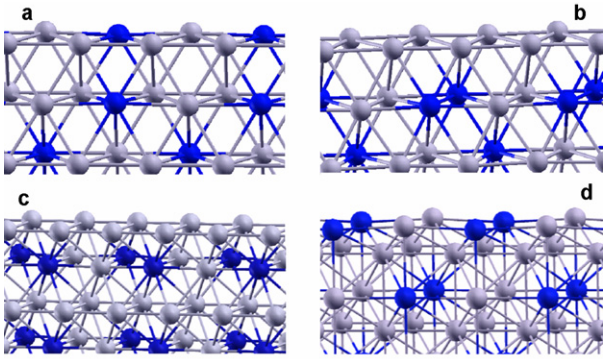

Figure 3. (a) Bulk-truncated and (b) experimentally found energetically favored arrangement for the $CoPt_3$ (111) facet. (c) Energetically favored (001) and (d) (110) facets (see text for details). Blue (dark) spheres denote Co atoms, gray (light) ones denote Pt atoms.

The same argument applies to the study of the $CoPt_3(110)$ facet (see figure 3(d)). A peculiar behavior was observed in general for the $CoPt_3(110)$ facet, for which the bulk-truncated termination can be either a pure Pt or a half-Pt–half-Co facet. Experiments have shown that the Co-rich facet is actually the energetically preferred one [36]. We also confirmed this experimental evidence by performing calculations with slabs that had different Co and Pt surface terminations.

We report in first three rows of table 1 the relaxations (with respect to the ideal bulk-truncated one) of the surface layer and of the second and third layers, for the three high symmetry (111), (001) and (110) facets in $CoPt_3$. The (111) facet has an inward relaxation for both the surface ($\Delta d_1 = -0.3\%$) and the subsurface layer ($\Delta d_2 = -3.1\%$), and a similar behavior is seen for the (001) facet ($\Delta d_1 = -4.6\%$ and $\Delta d_2 = -3.8\%$), while the (110) facet shows the most common metallic behavior of an alternating layer relaxation (inward–outward–inward) [58–60] and the largest relaxation values (-15.6%, $+8.4\%$, -2.2% for the first three layers). This remarkable relaxation is clearly connected to the lowest stability of the (110) facet.

By using slabs of increasing thickness to ensure convergence on surface energy, we computed the surface energies for the three orientations for both the experimentally

Table 3. Adsorption energies for a single Au atom (1 Au) and for an Au atom in an adsorbed Au monolayer (1 ML) on $CoPt_3$ (111), (001) and (110) facets, respectively. The energies have been calculated with respect to that of an isolated Au atom and in the case of 1 ML also to that of an Au atom in a bulk Au crystal (the latter data are reported in brackets). The second column reports the distance between the gold atoms and the $CoPt_3$ surface for each of the cases studied.

	E_{ads} (eV)	$d_{Au-surf}$ (Å)
1 Au/$CoPt_3$(111)	3.09	2.11
1 Au/$CoPt_3$(001)	4.21	1.84
1 Au/$CoPt_3$(110)	4.46	1.40
1 ML Au/$CoPt_3$(111)	4.55 (0.13)	2.43
1 ML Au/$CoPt_3$(001)	4.70 (0.28)	2.12
1 ML Au/$CoPt_3$(110)	4.79 (0.37)	1.40

found most stable termination (table 2, first row) and the least stable one (according to our calculations, see table 2, second row). The results of our calculations for $CoPt_3$ show that the close-packed (111) facet is clearly the most stable one ($\sigma = 0.110$ eV Å^{-2}), while we have a small indetermination in defining the least stable one, whether this is the (110) or the (001) one. According to the results of our calculations so far, the two latter facets should react more easily with adsorbate atoms than the (111) facet.

We note that spin polarization was taken into account in these calculations. For the various facets we also carried out calculations without including the spin, with slabs thickness from five up to nine layers, in order to estimate the effect of spin polarization on the various surface energies. In the case of $CoPt_3$(111), these were practically the same in both cases ($\sigma_{CoPt_3}(111) = 0.11$ eV Å^{-2}) and therefore for this stable facet the inclusion of the spin in the calculations did not appear to affect the surface energy. Calculations including spin yielded indeed larger absolute values in energy (by 0.07 eV/atom) with respect to those without spin; however, the energy difference between slabs and bulk systems, which is finally related to the surface energy, was poorly affected by the spin polarization. Similar calculations have been reported for instance on nickel [42], and have equally shown that the effect of magnetization is certainly relevant for the absolute values of DFT total energies, but can be neglected when energy differences are involved.

We found the same negligible effect on the surface energy for the (001) facet, while on the other hand the inclusion of spin appeared to be of fundamental importance to correctly identify the most stable atomic surface configuration for the (110) facet. Our paramagnetic calculations wrongly predicted that the more stable bulk-truncated (110) termination is the Pt-rich one, while the inclusion of spin polarization yielded comparable values of surface energies for the Pt-rich and for the Co-rich facets. This latter result is somehow closer to the experimental evidence, according to which the Co-rich facet is actually the most stable configuration [36]. The difficulty in predicting correctly the properties of the (110) facet is probably connected to its comparatively lower stability. Substitutional processes and surface segregation therefore appear remarkably sensitive to the magnetic properties of materials [61].

Finally, we calculated surface energies for the (111), (001) and (110) bulk facets of gold. The results are reported in table 2 (third row). The (111) facet is again the most stable one[2], with $\sigma = 0.069$ eV Å^{-2}, while the (110) facet is the least stable one ($\sigma = 0.088$ eV Å^{-2}). These results are in good agreement with both experimental data (table 2, fourth row) and previous calculations [46, 62, 63] (table 2, fifth row).

4.2. Adsorption of Au on $CoPt_3$

Concerning the study of the Au–$CoPt_3$ interface, we first consider the adsorption of a single gold atom on the various $CoPt_3$ facets (since this can be viewed as the initial stage of Au growth on $CoPt_3$) and then the adsorption of 1 ML of gold. We chose as the favorite adsorption site for each facet a hollow site, i.e. the one that should be occupied instead either by a Co or a Pt atom in homoepitaxial growth.

In table 3 the adsorption energies for a single gold atom (first three rows) and for a gold atom embedded in 1 ML (last three rows) on $CoPt_3$ facets are reported. Adsorption energies are computed with respect to the case of an isolated Au atom in vacuum, and for the case of 1 ML we also report in brackets the absorption energies with respect to one Au atom in a bulk crystal. The last column of table 3 reports the distances of Au from the surface. These data show that the growth of atomic gold occurs preferentially on the (110) facet of $CoPt_3$, which has the highest binding energy ($E_{ads} = 4.46$ eV) and the lowest Au–substrate bond length ($d_{Au-surface} = 1.40$ Å) among all facets. The large binding energy for the (110) facet is related to the low stability of this facet (table 2, first row). The same considerations also apply when a whole monolayer of gold is deposited on the facet. The (110) facet has the highest binding

[2] We note that the theoretical value reported in [46] for the Au(111) surface energy underestimates the experimental one due to the use of a gradient corrected functional instead of the local one used in this work.

Table 4. Magnetic moments (in μ_B) from Lowdin analysis for hcp-Co, fcc-Co and Co and Pt atoms in $CoPt_3$. Grids of $24 \times 24 \times 24$ k-points for the fcc structure and $24 \times 24 \times 15$ for the hcp structure have been used for evaluating the magnetic moments. Our results are compared with corresponding values from the literature. If not otherwise specified, calculations are LDA, spin polarized and scalar relativistic.

	Co hpc	Co fcc	Co ($CoPt_3$)	Pt ($CoPt_3$)
LDA (GGA) this work	1.57 (1.71)	1.56 (1.76)	1.74 (1.93)	0.45 (0.55)
FLAPW [68]	1.65		1.70	0.30
LMTO [68]	1.57–1.60			
KKR full rel [67]	1.59–1.61	1.59	1.82	0.26
FPLMTO full rel (GGA) [52]			1.82 (1.89)	0.22 (0.24)
LSW [44]			1.69	0.27
Exp. [52, 66–68]	1.52–1.61		1.64	0.26

energy ($E_{ads} = 4.79$ eV with respect to an isolated Au atom or 0.37 eV with respect an Au atom in a bulk Au crystal) among all facets.

4.3. Au/$CoPt_3$ interfaces

We now turn to the main topic of this work, which is the study of the Au/$CoPt_3$ epitaxial interfaces. The structural relaxations of the three $CoPt_3$/Au interfaces are reported in table 1, rows 4 to 6. The (110) interface undergoes a rather small rearrangement, much smaller than that of the corresponding (110) facet (table 1, third row). The relaxation of the (001) interface is on the other hand is rather similar to that of the corresponding (001) facet. Finally, the (111) facet shows an enhanced relaxation when Au is adsorbed on it.

The $CoPt_3$–Au interfacial energies (γ) for the three orientations are reported in the last row of table 2. We recall that the same considerations made for the surfaces about the difficulty of determining quantities related to the stoichiometry for the (001) and (110) crystallographic orientations apply equally to the $CoPt_3$–Au interfaces.

The interfacial energy gives an estimation of energy required to create a unit area of interface. From the calculated values, we can infer that the (001) interface can be created quite easily, even with the formation of an alloy between Au and Pt (in this case the interfacial energy will have a negative value). Moreover, the formation of the (111) interface requires less energy than the (110) one. We cannot therefore exclude that, if the actual (001) γ is higher than 0.012 eV $Å^{-2}$, the (111) interface will be the most stable interface. This argument, based on equilibrium interfacial energies, is a simple non-dynamical description. After the first Au ad-layer deposition, the further Au growth (a kinetic process) is due to a complex balance between strain, adsorption energy of Au atoms on Au ad-layers, and competing effects by the surroundings (surfactants, precursors, temperature, structural relaxations and rearrangements due to nanodimensional effects).

5. Electronic and magnetic properties

5.1. Density of states

The relative stability of various analyzed surfaces and interfaces can be further discussed in detail by studying the electronic properties of the systems. The analysis of the density of states (DOS) is a well established tool by which it is possible to extract information on bond creation and electronic charge transfer, and thereby to study structure stability.

We can compare the DOS of $CoPt_3$ and Au bulk, surface and interface systems, in order to evaluate the effect of anisotropy on the electronic properties, and the interacting states at the interface between the two materials.

The vast majority of theoretical electronic studies on $CoPt_3$ have until now been focused on electronic and magnetic bulk properties, mainly in comparative studies of various alloy compositions, or of different alloys between Pt and magnetic elements [44, 64, 65], while few data have been reported for surfaces [57]. By comparing the DOS of $CoPt_3$ bulk (figure 4) with previous theoretical calculations [44, 65], we can see that

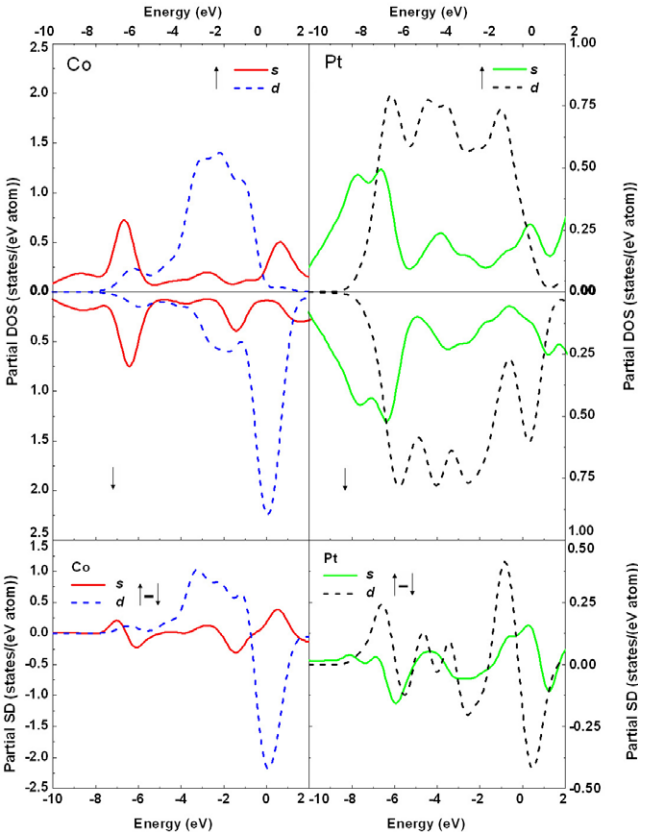

Figure 4. Upper two panels: PDOS for bulk $CoPt_3$, s- and d-states, majority and minority spin. Lower panels: partial spin density for bulk CoPt3, s- and d-states.

we obtain a good agreement in the shape and relative intensities of the curves. In particular, we note the presence of a minority spin peak, whose origin is due to the ferromagnetic character of the Co atom, at the Fermi energy. This feature, better highlighted in the spin density representation, is also present in the DOS of pure fcc-Co (not shown). In the alloy this peak is due to hybridization between the Co 3d and the Pt 5d bands, with also a minor contribution from s-electrons. The spin polarization induced on Pt is mainly due to the strong hybridization with Co d-states. The contribution of the Pt–Co s-states is mainly present at the lower edge of the d-band region, where the effect of magnetism is lower, as can be seen also for the low side (−4 to −7 eV) of the Pt d-band. The contribution of the Co d-band is stronger in the −4 to 1 eV region.

The PDOS of the three $CoPt_3$ facets are reported in figure 5. For the (111) and (001) facets, with Pt-rich terminations with respect to the bulk truncation, the main differences are located at Pt atoms of the first layer, with an overall shift of the DOS at higher energies, as expected, due to the lower surface stability with respect to the bulk phase, while Co atoms from the second layer show almost unaffected electronic properties. For the (110) facet, both Co and Pt atoms show variations in the electronic levels, in particular Pt has again a shift of electrons towards higher energies, while for Co both minority and majority peaks show an enhanced intensity.

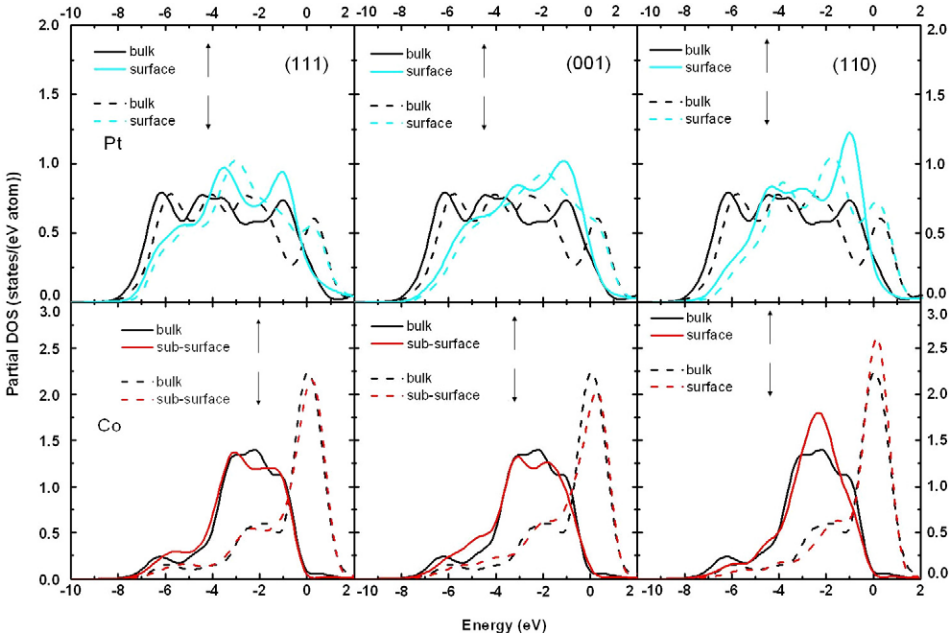

Figure 5. The d-PDOS resolved by atom (Pt in the upper panels, Co in the lower panels) and spin component (solid lines for majority spin, dashed lines for minority spin) of (111), (001) and (110) CoPt3 surfaces.

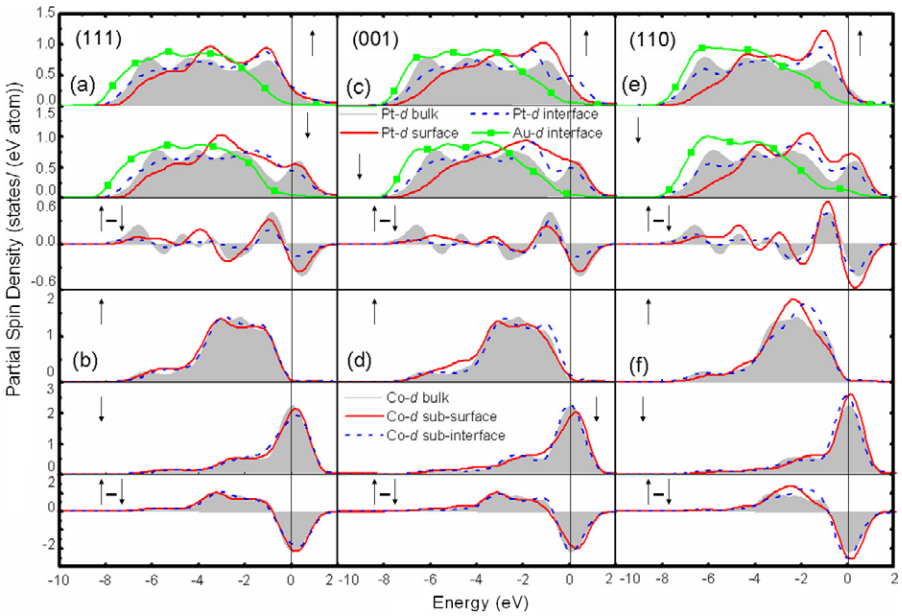

Figure 6. The d-PDOS of Pt (upper panels) and Co (lower panels) for (from left to the right) the (111) (panels (a) and (b)), the (001) (panels (c) and (d)) and the (110) (panels (e) and (f)) orientations. In each panel, the top graph report the majority DOS, the central graph the minority DOS, and the bottom graph the spin DOS. In each graph, the gray shaded area denotes the bulk reference DOS, the solid red curve the surface DOS, the dashed blue curve the interface DOS, and the solid green curve with squares the d-PDOS of Au at the interface.

We observe, in particular, a low-energy DOS depletion, while there is an increased DOS intensity at higher energy. This effect is dominant in Pt, and in Co for the (110) surface.

When considering the PDOS of atoms located at the interface, we observe, as a general trend, that the presence of adsorbed gold seems to stabilize the systems, with respect to the clean $CoPt_3$ surfaces, because of the reconstitution of a bulk-like termination, even if subject to strain and electronic bond differences. In figure 6, it is shown as the d-DOS of Pt interfacial atoms lies at lower energies with respect to the corresponding atom in the surface configuration. In the (110) interface, the resemblance between bulk and interface Pt atoms PDOS is even more evident. The hybridization between d-Au deep valence electrons and d-Pt states is mainly located between -2 and -8 eV, while a stronger hybridization between s-Au, s-Pt and s-Co states (see figure 7), with well-defined structures, is observed in the conduction region (4–6 eV above the Fermi level).

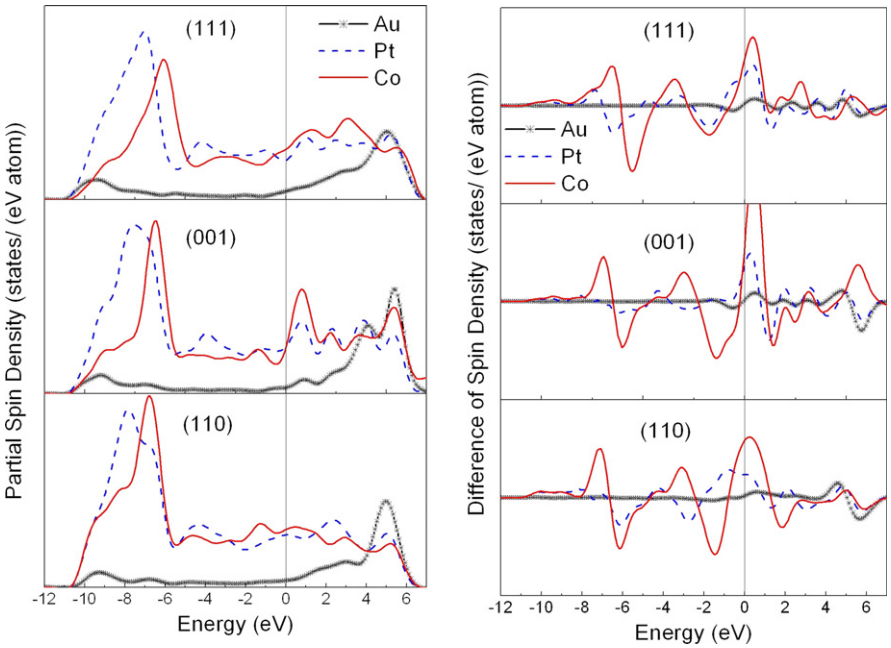

Figure 7. Left: s-PDOS of Au, Pt and Co for atoms located at the (111), (001) and (110) interfaces. Right: difference in spin density for the s-component of Au, Pt, and Co at the three interfaces.

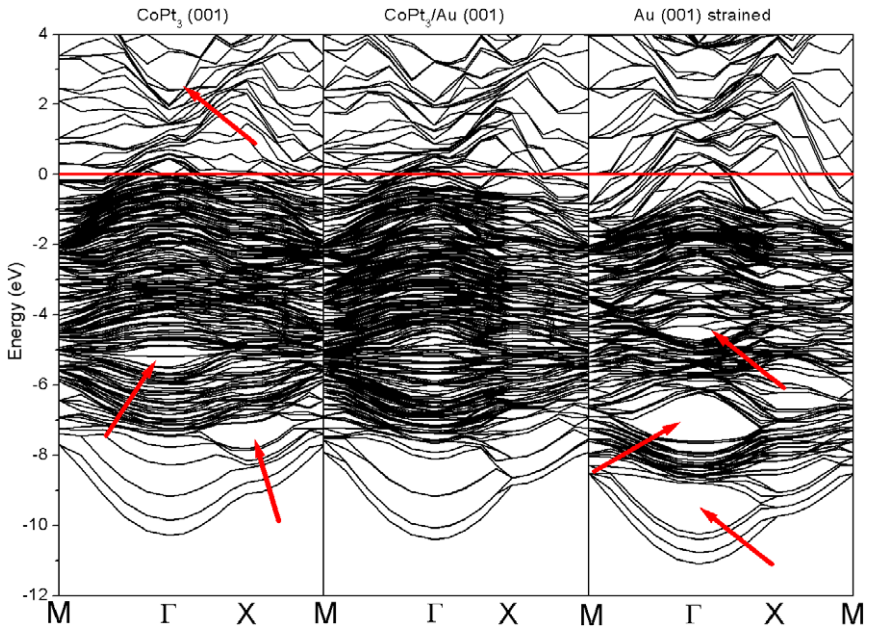

Figure 8. From left to right: electronic band structure of $CoPt_3$(001) surface, Au/$CoPt_3$(001) interface and Au(001) surface (with in-plane strain). Contributions are from both bulk and surface or interface layers. Red arrows denote the most important gaps in the band structure. Even if hybridized throughout the valence energy range, the d-contribution is more evident in the dense, flatter bands from −7 eV up to the Fermi level, while the s-contribution is dominant in the wide dispersion band at −8:−11 eV, and in the conduction region above Fermi energy.

The band structures reported in figure 8, together with the PDOS of figures 6 and 7, exemplify, for the (001) orientation, the effect of Au–$CoPt_3$ interfacial hybridization on the electronic states. The bulk *d*-PDOS of Au (not reported) is strongly localized in energy between −0.5 and −5 eV, and the effect of the surface anisotropy is mainly to delocalize this contribution on a broader range of energies (up to −9 eV for the strained system, see figure 7, and −10 eV for the real (001) surface, not reported), introducing some gaps due to both s- and d-orbitals (at −2:−4 eV, −7 eV and −9 eV). The interaction with the substrate does not simply re-create a bulk-like situation, but instead broadens the surface PDOS structures of gold, which is now strongly superimposed on the PDOS of the $CoPt_3$.

Some of the gaps in the band structure, present in both clean $CoPt_3$ and (strained) Au surfaces (red arrows in left and right panels of figure 8), are preserved, or slightly modified, in the final interface band structure, as the gap in s-states of Au at

Table 5. Magnetic moments (in μ_B) from Lowdin analysis for atoms from different layers at the three high symmetry interfaces.

	Co	Pt	Au
(111) layer 1	—	0.30	—
(111) layer 2	1.94	0.50	—
(001) layer 1	—	0.37	—
(001) layer 2	1.89	0.30	—
(110) layer 1	2.01	0.54	—
(110) layer 2	—	0.44	—
1 ML Au/(110)	1.80	0.33	0.06
Au/$CoPt_3$(110)	1.77	0.32	0.04
Au/$CoPt_3$(111)	—	0.25	0.01

Γ and −9 eV, or the gap at X and −7 eV (sd-states) in $CoPt_3$. In other cases, as for the gap at Γ and −7 eV in Au (sd-states), the strong overlap with sd-states from the alloy makes the gap disappear at the interface. The dispersion at the Fermi energy is also modified due to the interaction, with the dense d-band of $CoPt_3$ shifted towards lower energies.

5.2. Magnetic moments

In table 4 we report the calculated magnetic moments (from Lowdin analysis) for Co and $CoPt_3$ bulk materials and compare them with experiments and other works. From these data it is evident that the magnetic moment strongly depends on the method used (we are using pseudopotentials, instead of all-electron), on the exchange–correlation functional (LDA, GGA), and on the inclusion of full relativistic effects. The calculated μ_{Co} for fcc-Co is 1.56 μ_B and for hcp-Co it is 1.57 μ_B in good agreement with other results present in the literature.

Our results of magnetic moments and total magnetization for the $CoPt_3$ bulk per unit cell are $\mu_{Co} = 1.74\ \mu_B$, $\mu_{Pt} = 0.45\ \mu_B$ and $M_s = 3.02\ \mu_{B/\text{unit cell}}$, respectively (1.93, 0.55 and 3.28 in GGA), slightly higher than those reported by Kootte [44], which are 1.69 μ_B, 0.27 μ_B and 2.50 $\mu_{B/\text{unit cell}}$, respectively, and also higher than the experimental neutron diffraction results [66] (1.64 μ_B, 0.26 μ_B and 2.43 $\mu_{B/\text{unit cell}}$). The value for μ_{Co} is, however, lower than other theoretical results which include full relativistic corrections [52, 67]. Our value for μ_{Pt} is instead higher than all other reported results. We may hypothesize that the observed differences between our results and other data are mainly due to the use of the pseudopotential method. Moreover table 4 (first row) shows that the LDA performs much better than the GGA. In this work we are mainly interested in the effect of surface and interface geometries on the magnetism, which can be described quite accurately using LDA pseudopotentials.

Results for surfaces and interfaces are reported in table 5.

We verified that the magnetic moments from the inner layers of the slab converge to the bulk values. The Co magnetic moment at the surface is usually increased with respect to the bulk value in the hcp structure (1.57 μ_B) and in the fcc one. The magnetic anisotropy at the surface is induced by the large minority peak located at the Fermi energy in the DOS of Co.

We observe a small induction of magnetism in gold at the interface, due to hybridization between noble metal bands, and mainly directly induced by Co. The effect on gold is indeed larger at the (110) interface, where Co and Au can directly interact.

6. Discussion

The computed $CoPt_3$/Au interfacial energies (for which no theoretical or experimental data are available in the literature) lie in between the relatively small values found for several semiconductor interfaces and the much larger values found in *ab initio* calculations for other types of interfaces, such as for instance the Cr/Fe system [69]. Just to mention recent *ab initio* results, a typical semiconductor interface such as PbTe/CdTe [5] is characterized by $\gamma = 0.012$ eV Å^{-2}, whereas for the Fe/VN [19] interface γ could be as high as 0.035 eV Å^{-2}. As another example, for ZrO_2/Si a range of interfacial energy values were reported, [4] which depended on the interfacial structure and which could be as high as 0.08 eV Å^{-2}. The Cr/Fe interface on the other hand has a work of adhesion [69] equal to 0.335 eV Å^{-2}, which is a rather large value and is probably due to a strong mixing of d-orbitals and magnetic effects.

Our results show that for both Au and $CoPt_3$ the (111) facet is the most stable one (see table 2). The (111) $CoPt_3$ facet therefore should not promote the starting adsorption process of the first Au atoms. Such a process should be more favored on the (001) and (110) facets, for which we found the highest adsorption energy both for a single gold atom and for an Au monolayer (see table 3). This situation can be explained in terms of structural–electronic properties, due to the fact that the gold s–d shell induces a larger fcc lattice parameter with respect to the magnetic alloy. Gold atoms therefore prefer, as starting adsorption sites, the geometry configurations that guarantee more space to allocate their electronic cloud, which is the (110) hollow site, and, in second place, the (001) hollow site. The (111) $CoPt_3$ facet is the least suited to host gold atoms.

The equilibrium situation for these magnetic–metal interfaces, however, is slightly different. The interface presenting the lower value of γ is (001); however, the γ for the (111) face falls perfectly in the range of allowed values for the (001). The (110) interface requires, even with the lower obtained value for γ, a higher energy to be created than the (111).

The energetic considerations discussed so far should be carefully balanced, however, when examining the experimental results of Au growth on top of $CoPt_3$ nanocrystals. One point that deserves particular attention is that, due to the high symmetry of the fcc structure, a high selectivity in the growth of Au on a specific facet of $CoPt_3$ should lead to the formation of multiple domains on a single $CoPt_3$ nanocrystal, due to the presence of several equivalent facets, at least in the presence of large numbers of Au atoms. This, however, was not observed in our previous experiments [22], and it is also in contrast with several recently reported cases of nanocrystals made of other combinations of materials, such as for instance the hybrid Ag–Se [70] and Au–PbSe nanocrystals [71], in which multiple domains grew on top of starting nanoparticles, or of cases in

which a multi-crystalline shell could be grown on top of a given nanocrystal core under specific sets of conditions [32–35, 72]. A possible reason for the formation of a heterodimer in $CoPt_3$–Au nanocrystals is that the nucleation of a first Au domain on a given site on the surface of the starting $CoPt_3$ nanocrystal could trigger a self-catalytic reaction, so that further adsorption of Au atoms to that domain might be largely more favorable than on any other region on the nanocrystal surface. A similar mechanism might have been responsible for the formation of other types of nanocrystal heterodimers reported so far [72]. It might also be possible that the initial nucleation of more than one domain on a $CoPt_3$ nanocrystal would rapidly lead to a fast intra-particle Ostwald ripening process (as recently observed in CdSe–Au nanocrystals [73]) or to a coalescence of these domains on the surface of the $CoPt_3$ nanocrystals via their rapid migration and fusion. Unfortunately, nanocrystal species corresponding to the early stage of these hypothetical processes (i.e. nanocrystals characterized by the presence of multiple Au domains), could never be observed in the experiments [22] Finally, one cannot exclude the presence of a thin (1 ML or less) oxide layer on top of the $CoPt_3$ nanocrystals, which is difficult to identify experimentally and which could complicate matters further.

It is also important to remark that the calculations reported in this work mimic an infinite, perfect surface or interface, and thus a direct comparison with the properties of nanocrystals prepared by chemical synthesis needs to be made with great care. We are not dealing in our calculations with facets passivated with organic molecules such as the surfactants used in the growth of colloidal $CoPt_3$ nanocrystals or those involved in the formation of $CoPt_3$–Au nanocrystal dimers [22]. In that case, surfactant molecules could alter the relative stabilities of the various facets in a way that might be difficult to predict. However, the overall agreement with experimental trends in relative stabilities of the bulk facets and interfaces reported in the present study seems to indicate that the presence of surfactants should not modify the relative reactivities of the various facets dramatically.

Furthermore, the trends in relative stabilities of interfaces, and possibly in preferential growth of Au on certain $CoPt_3$ facets, could be different when Au grows on very small nanocrystals. In this case the (111) directions could be simply more exposed and less passivated by surfactant than other facets, hence the growth of Au would naturally take place preferentially along them. In addition, the substrate itself (i.e. the $CoPt_3$ nanocrystal), could easily absorb a significant portion of the strain (a lattice expansion should be less costly in a small nanocrystal than in a large one) so that the employed epitaxial model for the $CoPt_3$/Au interfaces might not be appropriate. However, concerning this last point, it is worth recalling a previously reported study of the Cu/Si interface [14], in which it was found that a strong expansion strain ($\sim$43%) applied to Cu, to obtain a coherent interface with Si, induced an overestimation of surface energy of just $\sim$3% with respect to the calculation including dislocation and misfit. We can therefore think that the $\sim$6% strain that we apply to the gold might not have much effect on the interfacial energetics in real cases.

7. Conclusions

In this work we report the first *ab initio* DFT theoretical description of energetics and electronics for the three high symmetry orientations of $CoPt_3$ alloy and Au/$CoPt_3$. We obtain a structural description for $CoPt_3$, in particular a surface stoichiometry, in good agreement with experiments for $CoPt_3$ surfaces, and we give the first estimation of surface energies σ for these systems. We also analyze the gold low coverage (up to 1 ML) and high coverage (a few MLs) adsorption on the magnetic alloy, which allowed us to determine the heterointerface geometries along different orientations between the magnetic alloy $CoPt_3$ and Au, and which allowed us to give the first estimation of interfacial energies γ for Au/$CoPt_3$.

The energetic data imply that the (110) clean surfaces are most reactive, and the (111) are most stable, and therefore adsorption of gold atoms is more efficient on the (110) alloy facet than on the (111) one. The further growth of gold under strain conditions imposed by the $CoPt_3$ substrate is favored on both (001) and (111) orientations, based on a thermodynamic analysis of interfacial energetics. In particular, the (001) interface has an even negative γ, connected to the possibility of Pt–Au alloying, and the (111) interface has lower interface energy than the (110) one, for each value of the Pt and Co chemical potential.

The analysis of electronic properties (DOS and band structure) and magnetic behavior provides a deep understanding of the magnetic–metal interaction. In particular, the overall effect of the interface formation is stronger on the Au than on the $CoPt_3$ DOS for atoms localized at the interface itself, and a large hybridization and mixing of states is realized both for s- and d-states.

As said in the introduction, this type of metal–magnetic interface is realized in colloidal heteronanostructures. However a direct comparison between theoretical modeling and such nanostructures is not straightforward and further experimental and theoretical work is required for a deeper understanding of the properties of these heteronanocrystals. Certainly strain, surfactants and solvent molecules, and kinetic factors, together with the finite size of the nanodimers, are expected to play an important role in the overall formation process of these heteronanocrystals.

Acknowledgments

We thank Dr Elvio Carlino for useful discussions. We thank the SPACI consortium and the initiative Progetti Calcolo Parallelo 2007 by CNR-INFM and CINECA for the allocation of computer resources. This work is partially funded by the European projects SA-NANO (contract no STRP 013698) and SPDIME (contract no STRP 029002).

References

[1] Bernardini F and Fiorentini V 1998 *Phys. Rev.* B **57** R9427–30
[2] Bernardini F, Fiorentini V and Vanderbilt D 1997 *Phys. Rev. Lett.* **79** 3958–61

[3] Dal Corso A, Posternak M, Resta R and Baldereschi A 1994 *Phys. Rev.* B **50** 10715–21
[4] Dong Y F, Feng Y P, Wang S J and Huan A C H 2005 *Phys. Rev.* B **72** 045327
[5] Leitsmann R, Ramos L E and Bechstedt F 2006 *Phys. Rev.* B **74** 085309
[6] Posternak M, Baldereschi A, Catellani A and Resta R 1990 *Phys. Rev. Lett.* **64** 1777–80
[7] Rao C N R, Vivekchand S R C, Biswasa K and Govindaraja A 2007 *Dalton Trans.* 3728–49
[8] Cozzoli P D, Pellegrino T and Manna L 2006 *Chem. Soc. Rev.* **35** 1195–208
[9] Lisiecki I, Filankembo A, Sack-Kongehl H, Weiss K, Pileni M P and Urban J 2000 *Phys. Rev.* B **61** 4968–74
[10] Dobrynin A N, Ievlev D N, Verschoren G, Swerts J, Van Bael M J, Temst K, Lievens P, Piscopiello E, Van Tendeloo G, Zhou S Q and Vantomme A 2006 *Phys. Rev.* B **73** 104421
[11] Fiorentini V and Methfessel M 1996 *J. Phys.: Condens. Matter* **8** 6525–9
[12] Noguera C, Finocchi F and Goniakowski J 2004 *J. Phys.: Condens. Matter* **16** S2509–37
[13] Feng J W, Zhang W Q and Jiang W 2005 *Phys. Rev.* B **72** 115423
[14] Wang X G and Smith J R 2005 *Phys. Rev. Lett.* **95** 156102
[15] Soon A, Todorova M, Delley B and Stampfl C 2006 *Phys. Rev.* B **73** 165424
[16] Christensen M, Dudiy S and Wahnström G 2002 *Phys. Rev.* B **65** 045408
[17] Christensen M and Wahnström G 2003 *Phys. Rev.* B **67** 115415
[18] Hartford J 1999 *Phys. Rev.* B **61** 2221
[19] Johansson S A E, Christensen M and Wahnström G 2005 *Phys. Rev. Lett.* **95** 226108
[20] Knizhnik A A, Safonov A A, Iskandarova I M, Bagatur'yants A A, Potapkin B V, Fonseca L R C and Stoker M W 2006 *J. Appl. Phys.* **99** 084104
[21] Wang S Q and Ye H Q 2006 *Curr. Opin. Solid State Mater. Sci.* **10** 26–32
[22] Pellegrino T, Fiore A, Carlino E, Giannini C, Cozzoli P D, Ciccarella G, Respaud M, Palmirotta L, Cingolani R and Manna L 2006 *J. Am. Chem. Soc.* **128** 6690–8
[23] Mornet S, Vasseur S, Grasset F and Duguet E 2004 *J. Mater. Chem.* **14** 2161–75
[24] Jun Y W, Choi J S and Cheon J 2007 *Chem. Commun.* 1203–14
[25] Gu H W, Yang Z M, Gao J H, Chang C K and Xu B 2005 *J. Am. Chem. Soc.* **127** 34–5
[26] Choi J S, Jun Y W, Yeon S I, Kim H C, Shin J S and Cheon J 2006 *J. Am. Chem. Soc.* **128** 15982–3
[27] Wang X, Kong X G, Yu Y and Zhang H 2007 *J. Phys. Chem.* C **111** 3836–41
[28] Peng X G, Schlamp M C, Kadavanich A V and Alivisatos A P 1997 *J. Am. Chem. Soc.* **119** 7019–29
[29] Dabbousi B O, RodriguezViejo J, Mikulec F V, Heine J R, Mattoussi H, Ober R, Jensen K F and Bawendi M G 1997 *J. Phys. Chem.* B **101** 9463–75
[30] Cao Y W and Banin U 2000 *J. Am. Chem. Soc.* **122** 9692–702
[31] Sashchiuk A, Langof L, Chaim R and Lifshitz E 2002 *J. Cryst. Growth* **240** 431–8
[32] Kim H, Achermann M, Balet L P, Hollingsworth J A and Klimov V I 2005 *J. Am. Chem. Soc.* **127** 544–6
[33] Lu W, Wang B, Zeng J, Wang X P, Zhang S Y and Hou J G 2005 *Langmuir* **21** 3684–7
[34] Tom R T, Nair A S, Singh N, Aslam M, Nagendra C L, Philip R, Vijayamohanan K and Pradeep T 2003 *Langmuir* **19** 3439–45
[35] Wang L Y, Luo J, Fan Q, Suzuki M, Suzuki I S, Engelhard M H, Lin Y H, Kim N, Wang J Q and Zhong C J 2005 *J. Phys. Chem.* B **109** 21593–601
[36] Shapiro A L, Rooney P W, Tran M Q, Hellman F, Ring K M, Kavanagh K L, Rellinghaus B and Weller D 1999 *Phys. Rev.* B **60** 12826–36
[37] Payne M C, Teter M P, Allan D C, Arias T A and Joannopoulos J D 1992 *Rev. Mod. Phys.* **64** 1045–97
[38] Franciosi A and VandeWalle C G 1996 *Surf. Sci. Rep.* **25** 1
[39] Kokalj A 2003 *Comput. Mater. Sci.* **28** 155
[40] Manna L, Wang L W, Cingolani R and Alivisatos A P 2005 *J. Phys. Chem.* B **109** 6183–92
[41] Rempel J Y, Trout B L, Bawendi M G and Jensen K F 2005 *J. Phys. Chem.* B **109** 19320–8
[42] Kalibaeva G, Vuilleumier R, Meloni S, Alavi A, Ciccotti G and Rosei R 2006 *J. Phys. Chem.* B **110** 3638–46
[43] Geisler A H and Martin D L 1952 *J. Appl. Phys.* **23** 375
[44] Kootte A, Haas C and Degroot R A 1991 *J. Phys.: Condens. Matter* **3** 1133–52
[45] Roques J and Anderson A B 2005 *Surf. Sci.* **581** 105–17
[46] Vargas M C, Giannozzi P, Selloni A and Scoles G 2001 *J. Phys. Chem.* B **105** 9509–13
[47] Hohenberg P and Kohn W 1964 *Phys. Rev.* **136** B864
[48] Kohn W and Sham L J 1965 *Phys. Rev.* **140** A1133
[49] Baroni S, Dal Corso A, de Gironcoli S and Giannozzi P, available online at http://www.pwscf.org/
[50] Perdew J P and Zunger A 1981 *Phys. Rev.* B **23** 5048
[51] Perdew J P and Wang Y 1992 *Phys. Rev.* B **45** 13244–9
[52] Galanakis I, Alouani M and Dreysse H 2000 *Phys. Rev.* B **62** 6475–84
[53] Tran F, Laskowski R, Blaha P and Schwarz K 2007 *Phys. Rev.* B **75** 115131
[54] Vanderbilt D 1990 *Phys. Rev.* B **41** 7892–5
[55] Dal Corso A, Pasquarello A, Baldereschi A and Car R 1996 *Phys. Rev.* B **53** 1180–5
[56] Saul A and Weissmann M 1999 *Phys. Rev.* B **60** 4982–7
[57] Ross P N 1992 *J. Vac. Sci. Technol.* A **10** 2546–50
[58] Wan J, Fan Y L, Gong D W, Shen S G and Fan X Q 1999 *Modelling Simul. Mater. Sci. Eng.* **7** 189–206
[59] Cho J H, Ismail, Zhang Z Y and Plummer E W 1999 *Phys. Rev.* B **59** 1677–80
[60] Methfessel M, Hennig D and Scheffler M 1992 *Phys. Rev.* B **46** 4816–29
[61] Müller S, Stühr M and Wieckhorst O 2006 *Appl. Phys.* A **82** 415–9
[62] Needs R J and Mansfield M 1989 *J. Phys.: Condens. Matter* **1** 7555
[63] Olivier S, Treglia G, Saul A and Willaime F 2006 *Surf. Sci.* **600** 1131–5
[64] Paudyal D, Saha-Dasgupta T and Mookerjee A 2004 *J. Phys.: Condens. Matter* **16** 2317–34
[65] Kashyap A, Garg K B, Solanki A K, Nautiyal T and Auluck S 1999 *Phys. Rev.* B **60** 2262–7
[66] Meninzer F and Paoletti A 1966 *Phys. Rev.* **143** 365
[67] Šipr O, Minár J, Mankovsky S and Ebert H 2008 *Phys. Rev.* B **78** 144403
[68] Iwashita K, Oguchi T and Jo T 1996 *Phys. Rev.* B **54** 1159–62
[69] Johnson D F, Jiang D E and Carter E A 2007 *Surf. Sci.* **601** 699–705
[70] Gao X Y, Yu L T, MacCuspie R I and Matsui H 2005 *Adv. Mater.* **17** 426–9
[71] Yang J, Elim H I, Zhang Q B, Lee J Y and Ji W 2006 *J. Am. Chem. Soc.* **128** 11921–6
[72] Yu H, Chen M, Rice P M, Wang S X, White R L and Sun S H 2005 *Nano Lett.* **5** 379–82
[73] Mokari T, Sztrum C G, Salant A, Rabani E and Banin U 2005 *Nat. Mater.* **4** 855–63